2004

Single-Kernel Maize Analysis by Near-Infrared Hyperspectral Imaging

Robert P. Cogdill
Duquesne University

Charles R. Hurburgh Jr.
Iowa State University, tatry@iastate.edu

Glen R. Rippke
Iowa State University

Stanley J. Bajic
Iowa State University

Roger W. Jones
Iowa State University, jonesrw@ameslab.gov

See next page for additional authors

Single-Kernel Maize Analysis by Near-Infrared Hyperspectral Imaging

Abstract

The objectives of this research were: (1) to develop a technique for creating calibrations to predict the constituent concentrations of single maize kernels from near-infrared (NIR) hyperspectral image data, and (2) to evaluate the feasibility of an NIR hyperspectral imaging spectrometer as a tool for the quality analysis of single maize kernels. Single kernels of maize were analyzed by hyperspectral transmittance in the range of 750 to 1090 nm. The transmittance data were standardized using an opal glass transmission standard and converted to optical absorbance units. Partial least squares (PLS) regression and principal components regression (PCR) were used to develop predictive calibrations for moisture and oil content using the standardized absorbance spectra. Standard normal variate, detrending, multiplicative scatter correction, wavelength selection by genetic algorithm, and no preprocessing were compared for their effect on model predictive performance. The moisture calibration achieved a best standard error of cross-validation (SECV) of 1.20%, with relative performance determinant (RPD) of 2.74. The best oil calibration achieved an SECV of 1.38%, with an RPD of only 1.45. The performance and subsequent analysis of the oil calibration reveal the need for improved methods of single-seed reference analysis.

Authors

Robert P. Cogdill, Charles R. Hurburgh Jr., Glen R. Rippke, Stanley J. Bajic, Roger W. Jones, John F. McClelland, Terrance C. Jensen, and Junhong Liu

SINGLE-KERNEL MAIZE ANALYSIS BY NEAR-INFRARED HYPERSPECTRAL IMAGING

R. P. Cogdill, C. R. Hurburgh, Jr., G. R. Rippke

(2/2006) Discussion at Iowa State has led to a request to add authors to this article. The changed author list is: R. P. Cogdill, C. R. Hurburgh, Jr., G. R. Rippke, S. J. Bajic, R. W. Jones, J. F. McClelland, T. C. Jensen, J. Liu

ABSTRACT. *The objectives of this research were: (1) to develop a technique for creating calibrations to predict the constituent concentrations of single maize kernels from near-infrared (NIR) hyperspectral image data, and (2) to evaluate the feasibility of an NIR hyperspectral imaging spectrometer as a tool for the quality analysis of single maize kernels. Single kernels of maize were analyzed by hyperspectral transmittance in the range of 750 to 1090 nm. The transmittance data were standardized using an opal glass transmission standard and converted to optical absorbance units. Partial least squares (PLS) regression and principal components regression (PCR) were used to develop predictive calibrations for moisture and oil content using the standardized absorbance spectra. Standard normal variate, detrending, multiplicative scatter correction, wavelength selection by genetic algorithm, and no preprocessing were compared for their effect on model predictive performance. The moisture calibration achieved a best standard error of cross-validation (SECV) of 1.20%, with relative performance determinant (RPD) of 2.74. The best oil calibration achieved an SECV of 1.38%, with an RPD of only 1.45. The performance and subsequent analysis of the oil calibration reveal the need for improved methods of single-seed reference analysis.*

Keywords. Imaging, Maize, Near-infrared (NIR), Single-seed analysis, Spectroscopy.

Near-infrared spectroscopy (NIRS) has quickly evolved from a laboratory technique into a mainstay tool for a variety of qualitative and quantitative analysis tasks. The analytical capabilities of NIRS rely on the broad and repeating absorption bands of carbon-hydrogen, oxygen-hydrogen, and nitrogen-hydrogen bonds. While the overlapping of absorption bands makes direct interpretation of absorption spectra difficult, chemometric techniques, such as partial least squares (PLS) regression, can be used to produce accurate calibration equations for many constituents and quality attributes with little or no sample preparation (Osborne et al., 1993).

Whole-grain NIRS analyzers have been calibrated for the prediction of constituents such as moisture, crude protein, starch, fiber, and oil content in maize, soybeans, and wheat (Hardy et al., 1996). An NIR bulk-grain analyzer predicted the Roundup Ready status of whole soybeans (Roussel et al., 2001). The growing demand for specific quality traits in grains and oilseeds has led the seed-breeding industry to adopt NIRS analysis for research and development.

Non-destructive bulk-grain analyzers have been used as a segregation tool for breeder seed. The higher-quality groups are planted, while the lower-quality groups are discarded, which speeds the introduction or enhancement of valuable quality traits. Intuitively, the ability to analyze smaller samples of grain will yield greater increases in quality per selection generation, since fewer low-quality seeds will be planted in each group. Silvela et al. (1989) demonstrated that the rate of oil content gain was significantly greater if breeding selection occurred on a single-kernel basis, as opposed to composite samples containing all kernels on an ear.

NIRS single-seed quality analysis has been applied to predict oil and protein content in maize, wheat, and soybeans (Orman and Schumann, 1992; Abe et al., 1995); moisture content in maize, lima beans, peanuts, soybeans, and sunflower (Norris and Hart, 1965; Finney and Norris, 1978; Norris, 1983; Lamb and Hurburgh, 1991); oil content in meadowfoam (Patrick and Jolliff, 1997); oleic and linoleic acid in sunflower (Sato et al., 1995; Velasco et al., 1999a); and oil, protein, glucosinolate content, and oleic, linoleic, and erucic acid concentration in rapeseed (Sato et al., 1998; Velasco et al., 1999b; Velasco et al., 1999c).

Seed orientation affects the accuracy of single-seed analysis using traditional NIR spectrometers (Orman and Schumann, 1992; Abe et al., 1995). In unpublished comments, some maize breeders have also mentioned poorer repeatability of single-kernel NIRS analyses using conventional means. In their work, Finney and Norris (1978) suggest that the inability of (non-imaging) NIR spectrometers to capture internal constituent gradients within maize kernels leads to discrepancies between predicted and measured composition. It has been theorized that the analyzer sees only

The authors are **Robert P. Cogdill,** Graduate Research Assistant, Graduate School of Pharmaceutical Sciences, Duquesne University, Pittsburgh, Pennsylvania; **Charles R. Hurburgh, Jr., ASAE Member Engineer,** Professor, Agricultural and Biosystems Engineering Department, Iowa State University, Ames, Iowa; and **Glen R. Rippke,** Laboratory Manager, Agricultural and Biosystems Engineering Department, Iowa State University, Ames, Iowa. **Corresponding author:** Charles R. Hurburgh, Jr., Agricultural and Biosystems Engineering Department, 1541 Food Sciences Building, Iowa State University, Ames, IA 50011; phone: 515-294-8629; fax: 515-294-6383; e-mail: tatry@ iastate.edu.

a small portion of kernels, which are very heterogeneous in composition. NIRS imaging may be more suitable for quantifying the spectral characteristics of spatially heterogeneous materials (such as single kernels of maize), since it sees the entire kernel at once.

HYPERSPECTRAL NIRS IMAGING

Hyperspectral NIRS imaging is a form of NIRS imaging that captures images at many wavelength bands in the NIR region. Hyperspectral NIRS imaging is an extension of multispectral NIRS imaging, where images are captured at a much smaller number of wavelength bands (usually two or three). Image data collected by a hyperspectral imaging system are arranged into a three-way array of data, called a hypercube. The first two (x and y) axes of the array are vertical and horizontal pixel coordinates. The third (z) axis is the spectral dimension. For example, a hyperspectral imaging system with a 512×512 pixel detector array that sampled 69 wavelengths would collect 262,144 spectra during each analysis, in a $512 \times 512 \times 69$ array. Because of the vast amount of information collected, it is important to establish reasonable levels of spatial and spectral resolution as a trade-off between accuracy and computing time for any practical application of hyperspectral NIRS imaging.

NIRS imaging of agricultural biomaterials has been used for quality control and defect detection in apples (Bellon et al., 1992; Upchurch et al., 1994), peaches and apricots (Miller and Delwiche, 1990; Zwiggelaar et al., 1996), beef (Hatem et al., 1999), and poultry carcasses (Park et al., 1998). Sugiyama (1999) designed a multispectral imaging system to predict the distribution of sugar in the cross-section of ripe melons. Ridgeway and Chambers (1998) used NIRS imaging to detect insects inside single kernels of wheat. Archibald et al. (1998) developed a system to analyze wheat protein and determine color classification on a single-kernel basis. Taylor and McClure (1989) used NIRS imaging to visualize plant stress in tobacco leaves, and Evans et al. (1998) used a hyperspectral NIRS imaging system to quantify nitrogen stress on growing green edible bean plants.

OBJECTIVES

The objectives of this work were:
- To develop a technique for creating calibrations to predict the constituent concentrations of single maize kernels from near-infrared (NIR) hyperspectral image data.
- To evaluate the feasibility of an NIR hyperspectral imaging spectrometer as a tool for the quality analysis of single maize kernels.

MATERIALS AND METHODS

SAMPLES

The objectives of the work were completed by developing exploratory calibrations to predict moisture and oil concentration in single kernels of maize using a hyperspectral imaging spectrometer. The imaging spectrometer worked by collecting images of the light diffusely transmitted through the kernels at NIR wavelengths. Transmittance was chosen, rather than reflectance, since it was expected that transmittance measurements would be less affected by sample positioning (i.e., which side of the kernel faces the detector).

Table 1. Summary of moisture and oil calibration dataset statistics.

	Moisture Calibration[a]		Oil Calibration[b]	
	All Data	Calibration Set	All Data	Calibration Set
Number of samples	495	473	168	151
Average	15.83	15.79	3.38	3.21
Maximum	30.46	30.46	12.16	12.16
Minimum	9.74	9.74	0.26	0.26
Standard deviation	3.39	3.29	2.17	1.99

[a] % moisture concentration (wet basis).
[b] % oil concentration ("as is" moisture basis).

The samples for the moisture and oil calibration datasets (table 1) were selected from the maize calibration sample library at the Grain Quality Laboratory of Iowa State University. Single-kernel moisture reference data were obtained from air-oven testing of kernels at 103°C for 72 h according to ASAE Standard S352.2 (*ASAE Standards*, 1997).

Oil reference chemistry data were obtained by supercritical fluid extraction (SFE) on the single-kernel samples using a Leco FastFat HT supercritical fluid extractor (Leco Corporation, St. Joseph, Mich.). Single kernels were crushed with mortar and pestle, weighed, and then placed in the SFE (AOCS, 1993) for oil extraction. The crushed kernel was weighed once more after extraction to calculate the mass of oil extracted. The oil calibration set was smaller than the moisture calibration set because the supercritical fluid extraction method was far more expensive and time consuming than the oven moisture determination.

HYPERSPECTRAL IMAGING SPECTROMETER

The imaging spectrometer consisted of a detector, tunable optical filter, sample stage, collimating optics, and light source (fig. 1). The detector was an Apogee KX-260 monochrome scientific camera (Apogee Instruments, Inc., Auburn, Cal.), which used a thermoelectrically cooled, 512×512 pixel, silicon CCD array. The imaged data were digitized to a quantization level of 14 bits by an on-board microprocessor. It was decided that a silicon detector should be used because of its combination of low price, availability, access to optical components and filters, and high quantum efficiency (QE) in the spectral range generally used for diffuse transmittance NIR measurements.

The tunable optical filter was a Varispec model VS-NIR liquid crystal tunable filter (LCTF) with the following specifications: 55 mm clear aperture, 700-1100 nm tunable range. The bandwidth varies approximately proportional to the square of the center wavelength, and is specified as 10 nm at 850 nm center wavelength; the wavelength accuracy is defined as 1/8 of the actual bandwidth at the center wavelength selected (Cambridge Research and Instrumentation, Inc., Woburn, Mass.). An LCTF was chosen as the method of wavelength selection for its combination of high tuning speed, appropriate range, narrow bandpass, and ease of use (Miller and Hoyt, 1995; Archibald et al., 1998; Evans et al., 1998).

The light source, a 250 W, 24 V tungsten-halogen lamp, was powered by a DC source to minimize (60 Hz) noise. The collimating optics consisted of a 700 nm long-pass filter (to reduce the effects of out-of-band light), a focusing lens, a diffuser, and a flat mirror that directed the light through the
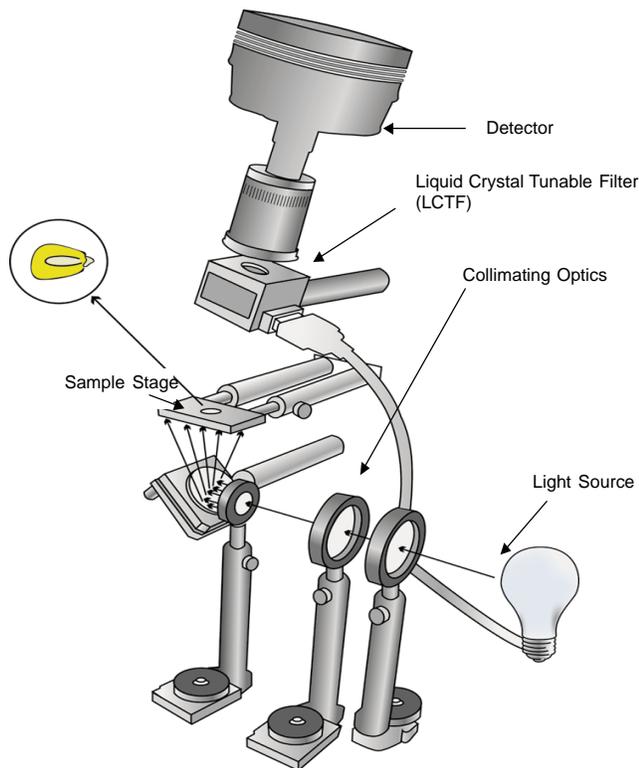
Figure 1. Hyperspectral imaging spectrometer.

sample presentation stage. The sample presentation stage consisted of a silica glass microscope slide mounted on a stable frame.

During sample analysis (image acquisition), a single kernel of maize rested freely on the microscope slide. An average-sized kernel covered approximately 60,000 pixels (approximately 23% of the detector area). Preliminary experiments showed no significant, systematic relationship between kernel positioning and the quality or repeatability of the acquired spectra. Thus, the kernels were intentionally placed flat-side down (with the germ up or down) on the viewing stage, randomly positioned within the field of view.

The uniformity of the illumination was maximized by varying the relative positions of the focusing lens and the diffuser. The LCTF and camera were positioned at a small angle, as close to vertical as possible, so that the camera did not view the illumination beam directly (which would cause CCD saturation and pixel blooming). Thus, only light that had been diffusely transmitted by the kernel would reach the CCD detector.

The imaging equipment was controlled by custom-written software (Liu, 2001) that operated the LCTF and camera simultaneously. Processing of the image data and the chemometric modeling were implemented using the Image Processing Toolbox (The Mathworks, Inc., Natick, Mass.), the PLS_Toolbox 2.0 (Eigenvector Research, Inc., Manson, Wash.), and other custom-written MATLAB functions.

IMAGE ACQUISITION AND PREPROCESSING

Images were collected at 5 nm intervals, from 750 to 1090 nm, making a total of 69 images per kernel. The sampled wavelength range was chosen to encompass the usable range of the equipment and the normal wavelength

range for NIR measurements in the transmittance mode. The exposure time was varied by wavelength to compensate for changes in the detector sensitivity. The desired reference intensity was an average of 10,000 A/D counts (out of a possible 16,383 for a 14-bit camera) within a 200×200 pixel region in the center of an opal glass reference sample. Depending on the selected exposure time curve, approximately 90 s were required to collect the images for a complete hypercube.

For each kernel analyzed, two extra images were collected to construct a binary mask, which delineated the perimeter of the kernel. With a kernel placed upon the sample stage, one image was collected with, and the other without, a piece of opal glass placed beneath the sample stage. The absolute value of the arithmetic difference between these two images was used to set pixels (outside kernel periphery) to logical zero, while pixels corresponding to valid spectral data were set to logical one. The masked pixel data were unfolded into a two-dimensional array (Geladi and Grahn, 1996) of size $N \times 71$ prior to standardization and modeling (where N is the number of valid pixels).

A set of standardization images was acquired during every data collection session (i.e., each time the imaging spectrometer was re-started); in general, 10 to 20 kernels were scanned per session. The standardization images were intended to compensate for differences in the spectrometer's response across the field of view and across the spectral range. Three types of standardization images were collected: light, empty stage, and dark current. The light and empty stage references were collected at every wavelength sampled, while the dark current image was collected with the lens cap on (since it was assumed that CCD thermal noise was independent of wavelength).

The light references were images of an illuminated piece of opal glass placed beneath the sample stage. The empty stage images were of the sample stage with the light source powered, but no sample, which left only stray light to reach the CCD detector. The empty stage images were subtracted from the sample images to remove instrumental baseline effects. Both the light reference and empty stage images were taken at the same wavelength and exposure times as the sample images. The standardization image set was applied to all N pixels in the hypercube according to the following formula:

$$I_{\lambda,n} = \left[C\left(S_{\lambda,n} - D_n\right) \div \left(L_{\lambda,n} - D_n\right)\right]$$
$$- \left[C\left(E_{\lambda,n} - D_n\right) \div \left(L_{\lambda,n} - D_n\right)\right] \qquad (1)$$

where

n = pixel index variable ($n = 1\ldots N$)
$I_{\lambda,n}$ = standardized transmittance intensity, pixel n, at wavelength λ
$S_{\lambda,n}$ = sample image, pixel n, at wavelength λ
$E_{\lambda,n}$ = empty stage image, pixel n, at wavelength λ
$L_{\lambda,n}$ = light reference image, pixel n, at wavelength λ
D_n = dark current image, pixel n
C = mean brightness level within a 100×100 pixel region in the center of ($L_{850,(1:N)}$ - $D_{(1:N)}$).

Following standardization, the arithmetic mean of the transmittance images was calculated over all N pixels, at each of the 69 wavelengths, to reduce the entire hypercube of data to a single transmittance spectrum. It was understood that a

significant amount of information contained in the spatial variation of intensity was being thrown away. For example, kernel morphology (shape, thickness) and edge effects were expected to influence the local quality of spectra within the hypercube. However, procedures to correct or mitigate such effects have yet to be developed.

Following the hypercube reduction, each transmittance spectrum was converted to absorbance units according to $A = \log(I^{-1})$, where I is the standardized spectrum of transmittance intensity, and A is the resulting absorbance spectrum. Some absorbance spectra are shown in figure 2. The abnormally large spectral noise is immediately apparent ($>10^{-2}$ AU) in the large amount of variation that appears at a much higher frequency than the chemically relevant absorbance bands; indeed, the noise observed was more than two orders of magnitude higher than is normally expected during NIR spectroscopy (typically $<10^{-4}$ AU). Since thousands of spectra are being co-added by averaging the pixels within each image plane, one would normally expect the signal-to-noise ratio to be much higher. However, a distinction must be made between the different sources of noise involved in this situation. If the dominant noise were shot noise (due to the relatively small electron well depth for each pixel) or readout noise, then averaging pixels would improve the signal-to-noise ratio. Because the imaging spectrometer requires a relatively large amount of time to collect a complete scan, the dominant noise sources were due to external factors varying in time (light source vibration and drift, stray light, LCTF variation, etc.), which can only be mitigated by co-adding multiple sets of exposures, or by some means of double-beam via a second (more stable) single-channel spectrometer, or by including internal references.

To correct for between-sample variations in pathlength, scatter coefficient, and other sample characteristics, as well as for variations in instrument response over time, spectral preprocessing methods (known to reduce such effects) were tested along with the calibrations. The standard normal variate (SNV) transformation, detrending (DET), and multiplicative scatter correction (MSC) were compared to assess their respective impact on model performance.

The SNV transformation (Barnes et al., 1989) is an intuitive choice for correcting the type of multiplicative and additive spectral effects that were expected:

$$SX = (X - x) / \sigma_x \qquad (2)$$

where

SX = SNV transform of X
X = spectrum (absorbance, transmittance, intensity, etc.)
x = mean of X
σ_x = standard deviation of X.

As can be seen (eq. 2), constant multiplicative or additive effects, such as pathlength and scattering variation, or instrument drift, should be removed using the SNV transformation. The SNV transformation requires few calculations, is relatively easy to understand, and often works well in practice. SNV cannot, however, correct non-constant (sloping or curving) baseline effects, and it may remove important information from (or even add noise to) the model in some situations. Detrending (Barnes et al., 1989) also removes additive baseline effects by subtracting from the spectrum a linear or polynomial fit of itself against the wavelength axis (or an index variable), but detrending is ineffective in removing multiplicative effects since no normalization is involved. Therefore, detrending is often used in conjunction with the SNV transformation.
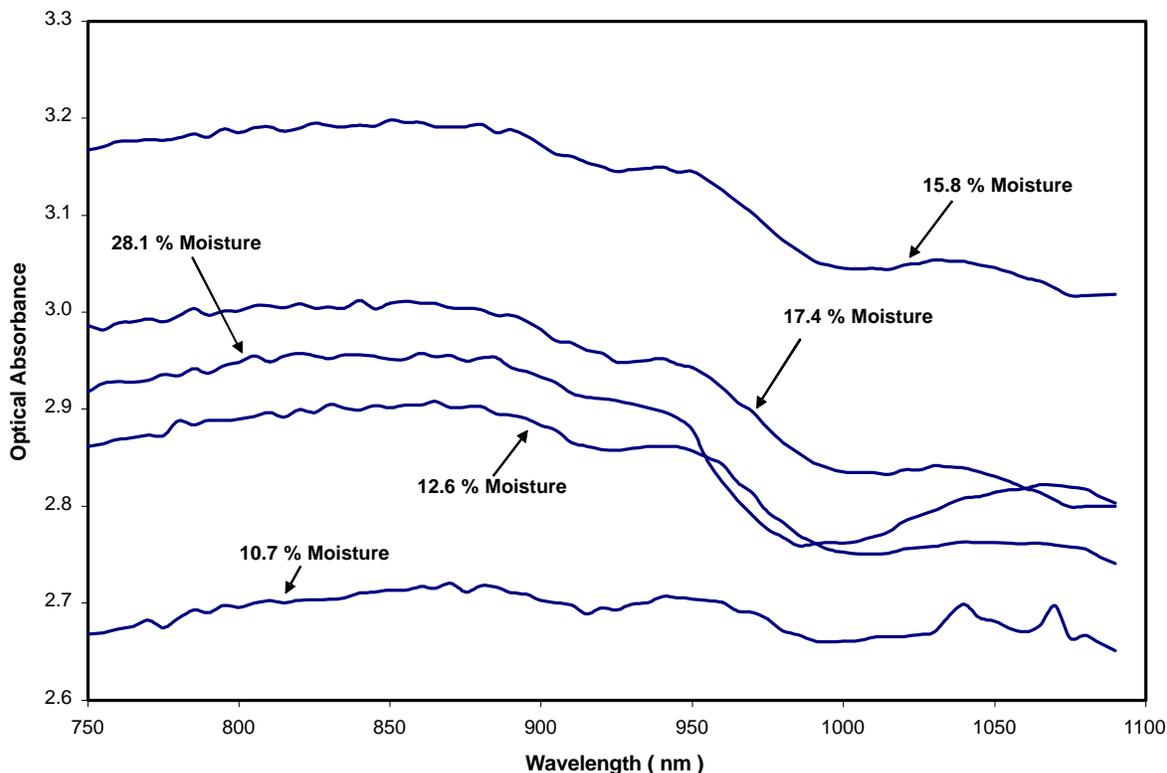

Figure 2. Absorbance spectra acquired from single kernels of maize using the hyperspectral imaging spectrometer.

Multiplicative scatter correction corrects multiplicative and non-constant (linear) additive baseline effects in a single step (Martens and Næs, 1989). MSC offsets and rotates each spectrum according to the inverse of a linear fit between the spectrum and a reference spectrum (in this case, the mean vector of the calibration databases). MSC often works well in practice, but it is greatly affected by spectral noise. The algorithms supplied by the PLS_Toolbox were applied for all preprocessing operations.

CALIBRATION DEVELOPMENT

Two multivariate regression algorithms were compared for the full-spectrum calibration tests: partial least squares (PLS) regression (Wold et al., 1984; Geladi and Kowalski, 1986; Martens and Næs, 1989) and principal component regression (PCR) (Næs and Martens, 1988; Martens and Næs, 1989). While both techniques are latent-variable regression techniques, it was anticipated that one or the other may have an advantage. Because PLS seeks to maximize the covariance between the predictor and predicted variables, poor quality reference data may lead to the derivation of factors correlated with erroneous reference data. On the other hand, since the factors derived by PLS are ordered according to decreasing covariance between predictor and predicted variables, using a PLS model should result in fewer latent variables being retained, hopefully increasing the signal-to-noise ratio of the model. Prior to deriving each regression, the spectra were mean-centered, and the reference data was mean-centered and scaled to unit variance to improve the condition of matrices for inversion.

During the initial steps of developing the moisture and oil calibrations, gross outliers were removed from the datasets. Gross outliers were identified according to their Hotellings T^2 distance from the center of the combined datasets, distance relative to confidence intervals in score plots, and level of prediction residuals. Both principal components analysis and PLS (without preprocessing) calculations were used to derive outlier limits and to identify outlying samples. Because preprocessing may have rendered some samples legitimate (which would have otherwise been deemed outlying), there may have been some benefit in culling the data independently for each preprocessing technique. However, to facilitate the comparison of results, outlying samples were identified and removed only once, with the reduced datasets being used for all subsequent models, except where indicated otherwise.

For all latent-variable models, optimal model parameters and prediction performance were estimated using 10-block cross-validation. During 10-block cross-validation, the calibration dataset is randomly broken into ten groups, and predictions for each of the ten groups are drawn using calibration equations calculated with the remaining nine groups of spectra. Ten iterations of each 10-block cross-validation run were performed. Thus, model performance is defined as the root mean squared error of prediction during cross-validation (SECV). Cross-validation is generally used as a tool to aid in determining model parameters (e.g., PLS factors) and for estimating the prediction error that would be expected when new samples are encountered.

Besides the accuracy of the calibrations, calibration stability was tested. To test calibration stability, a diverse set of 28 single-kernel samples was scanned, three times each (with repositioning for each scan), and a prediction was derived for each of the extracted scans using each of the calibrations. The root mean squared error (RMSE) between each sample's repeat predictions and their mean prediction was calculated for each calibration. Calibrations with a low RMSE between predictions should be more robust when applied to future samples not represented in the calibration dataset. Moreover, the RMSE was used to estimate the repeatability of the instrument for the purpose of error analysis.

WAVELENGTH SELECTION BY GENETIC ALGORITHM

A genetic algorithm (GA) search was used to identify an optimal subset of the original 69 wavelengths for chemometric modeling. The GA was to reduce the data and, hopefully, noise by omitting unnecessary wavelengths from the model. The GA is an adaptive search algorithm that imitates the genetic evolutionary process to efficiently solve complex combinatorial search problems. Genetic algorithms are efficient because they can avoid local minima while utilizing parallel exploration of the search space (Goldberg, 1989a; Tang et al., 2000).

The GA software provided by the PLS_Toolbox was used for wavelength selection. Implementing the GA required setting population size, window width, percentage of initial terms included, maximum generations, percentage of equal chromosomes at convergence, mutation rate, and the crossover setting. The population size was set to 68, the nearest setting to the chromosome length (Goldberg, 1989b). The window width was set to one, and the percent initial terms (starting number of wavelengths) was set at 30% (PLS_Toolbox default). The maximum generations (iterations) were set to 225 to provide enough opportunity for convergence. The percentage at convergence parameter, which stops the algorithm when a certain percentage of chromosomes (wavelength sets) in the current population have the same solution, was set to 70%. The mutation rate was set to 0.007, which is generally set in proportion with the population size (Goldberg, 1989a). The crossover parameter was set to double crossover. Multiple linear regression (MLR) and 10-block cross-validation were utilized as the cost function with the GA. Any preprocessing was performed on the complete spectrum prior to application of the genetic algorithm.

RESULTS AND DISCUSSION
MOISTURE CALIBRATION RESULTS

The results of the moisture calibration tests (table 2) suggest that little is to be gained by applying any of the preprocessing methods prior to moisture calibration, although applying the detrending operation may have some merit. MSC, however, was nearly useless on the noisy spectral data, requiring a significant number of samples to be removed before even relatively useful models could be derived. In light of this (and other experiences during this work), MSC was not used along with the GA, or for the oil calibration.

Table 2. Comparison of regression algorithms and preprocessing options using single-kernel moisture calibration dataset.

Model Basis		Preprocessing Applied					
		None[a]	None	SNV	DET	SNV-DET	MSC
PLS	Number of samples	495	473	473	473	473	457
	Factors	14	11	13	10	13	9
	r^2	0.786	0.871	0.836	0.872	0.828	0.664
	SEC[b]	1.17	1.05	1.07	1.04	1.07	1.64
	SECV[b]	1.91	1.20	1.36	1.20	1.35	1.95
	RPD[c]	1.78	2.74	2.42	2.75	2.43	1.70
	Stability[d]	0.94	0.87	1.18	0.88	0.18	1.04
PCR	Number of samples	495	473	473	473	473	456
	Principal components	9	17	14	16	14	13
	r^2	0.558	0.856	0.786	0.858	0.792	0.647
	SEC[b]	2.15	1.19	1.41	1.19	1.41	1.88
	SECV[b]	2.31	1.25	1.52	1.25	1.50	2.01
	RPD[c]	1.47	2.63	2.17	2.63	2.20	1.65
	Stability[d]	0.04	0.07	0.00	0.07	0.07	0.06
GA+MLR	Number of samples	495	473	473	473	473	- -
	Number of wavelengths	27	29	27	23	31	- -
	r^2	0.795	0.853	0.745	0.820	0.806	- -
	SEC[b]	1.39	1.15	1.43	1.24	1.28	- -
	SECV[b]	1.55	1.27	1.69	1.36	1.46	- -
	RPD[c]	2.19	2.59	1.94	2.41	2.25	- -
	Stability[d]	0.09	0.08	0.06	0.06	0.07	- -

[a] No outliers removed, models built using complete database.
[b] % moisture concentration (wet basis).
[c] Relative performance determinant = (standard deviation of reference chemistry / SECV).
[d] Root mean squared error (RMSE) of predicting repeatedly-scanned samples.
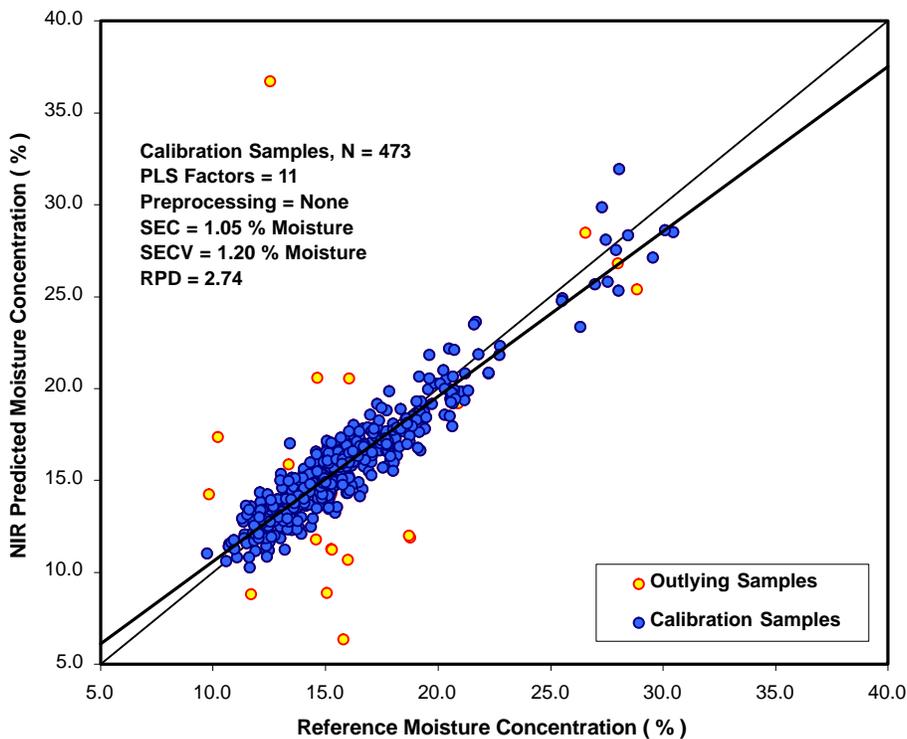
Figure 3. NIR predicted moisture concentration against the moisture reference chemistry.

Although the GA was able to improve the prediction performance in some cases, it was not able to produce the best models overall. Since the GA did not greatly reduce prediction performance, however, it may be advantageous to reduce the time of analysis.

The most accurate results were obtained using PLS on the raw absorbance spectra. With 11 factors included, the PLS calibration achieved an SECV of 1.2%, with an R^2 of 0.871 (fig. 3). In terms of RPD (standard deviation of reference
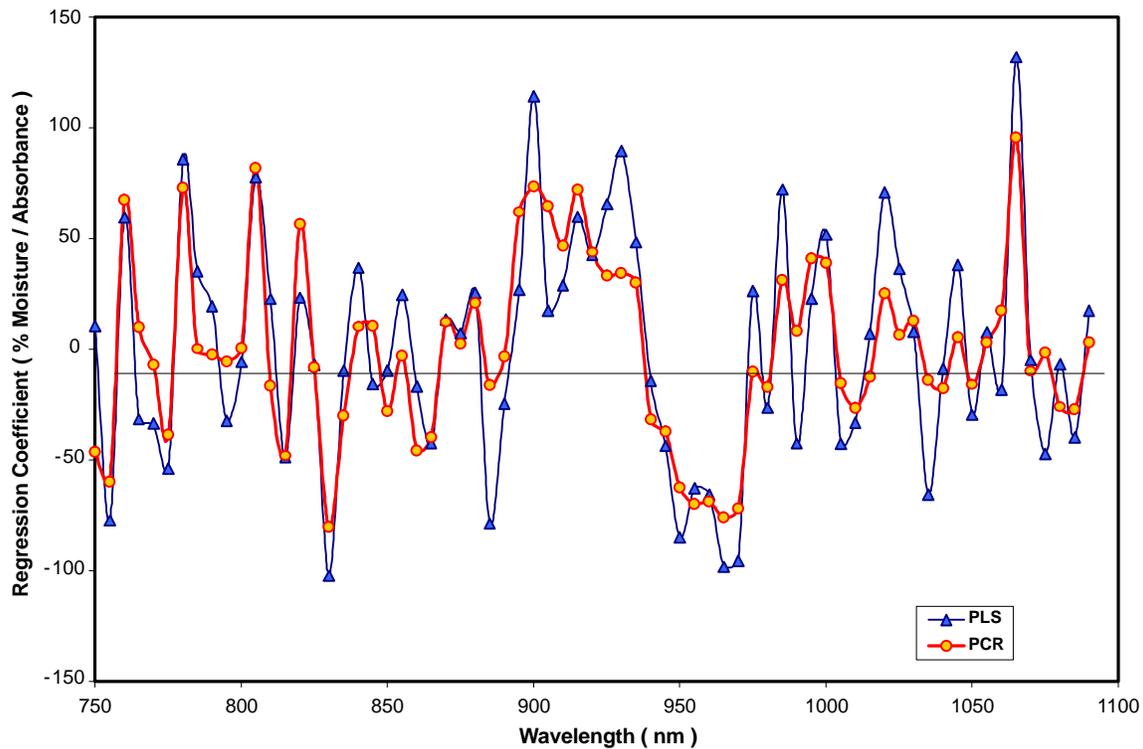
Figure 4. Moisture regression coefficient vectors derived using PLS and PCR. Although each performed essentially the same in prediction, the PCR calibration was more stable.
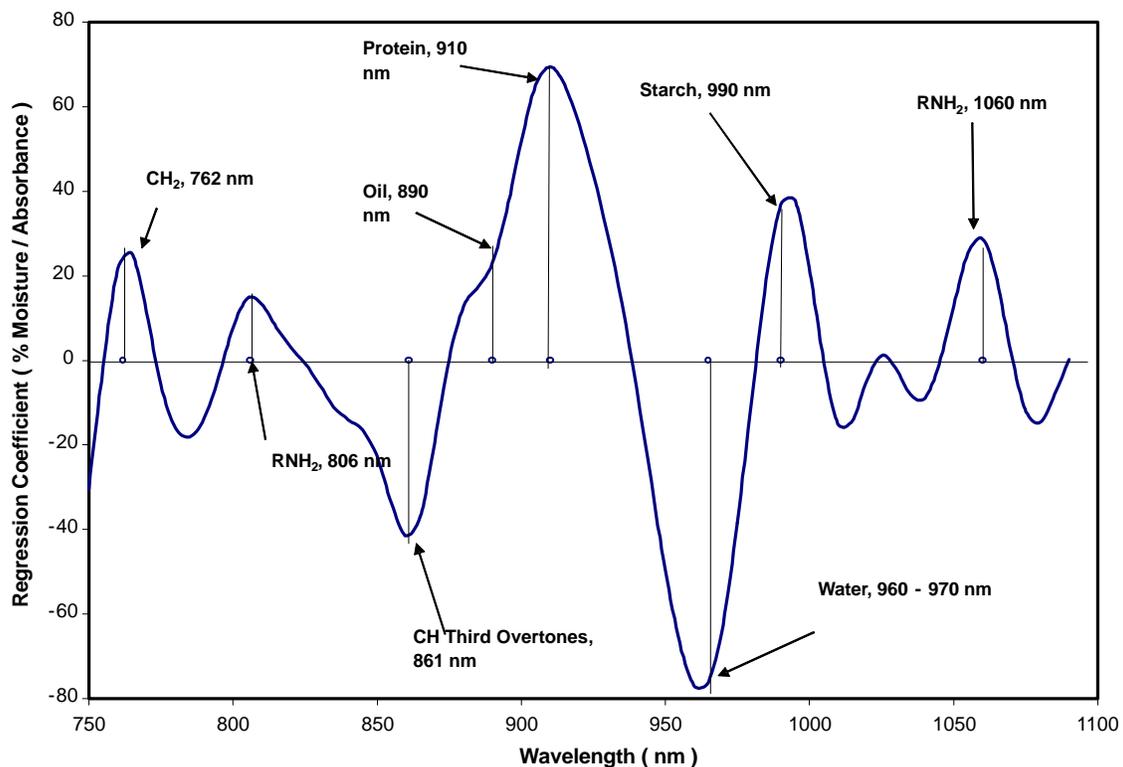

Figure 5. Moisture regression coefficient vectors derived using PCR, after adaptive smoothing. The locations of various overtone bands corresponding to major constituents in maize are shown.

values / SECV) (AACC, 1999), the calibration is at least able to distinguish between high and low moisture samples, but it is not likely useful for quantitative prediction since the SECV is greater than 40% of the total variation in the moisture reference data.

These results compare well with those of Finney and Norris (1978), who reported standard errors of prediction (SEP) between 2% and 3%. In their study, they developed single-kernel maize calibrations using a single-beam NIR spectrometer in the transmittance mode. They analyzed 392

Table 3. Comparison of regression algorithms and preprocessing options using single-kernel oil calibration dataset.

	Preprocessing Applied				
Model Basis	None[a]	None	SNV	DET	SNV-DET
PLS					
No. of samples	168	151	151	151	151
Factors	15	10	9	8	8
r^2	0.385	0.515	0.538	0.491	0.557
SEC[b]	1.18	1.09	1.09	1.15	1.10
SECV[b]	1.88	1.40	1.38	1.47	1.37
RPD[c]	1.15	1.43	1.45	1.36	1.46
Stability[d]	0.25	0.90	0.55	1.00	0.65
PCR					
No. of samples	168	151	151	151	151
Principal components	9	18	12	12	11
r^2	0.114	0.470	0.467	0.419	0.492
SEC[b]	1.88	1.19	1.26	1.33	1.25
SECV[b]	2.05	1.45	1.43	1.49	1.41
RPD[c]	1.06	1.37	1.40	1.34	1.42
Stability[d]	0.23	1.43	0.71	4.18	0.69
GA+MLR					
No. of samples	168	151	151	151	151
No. of wavelengths	25	22	23	26	25
r^2	0.439	0.508	0.454	0.407	0.554
SEC[b]	1.30	1.16	1.19	1.21	1.12
SECV[b]	1.62	1.41	1.50	1.56	1.39
RPD[c]	1.34	1.41	1.33	1.28	1.43
Stability[d]	0.36	0.84	1.80	2.23	0.83

[a] No outliers removed, models built using complete database.
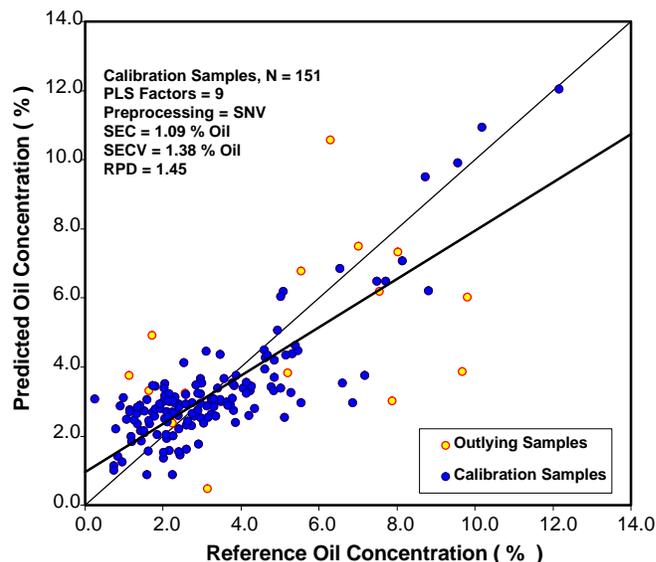[b] % oil concentration ("as is" moisture basis).
[c] Relative performance determinant = (standard deviation of reference chemistry / SECV).
[d] Root mean squared error (RMSE) of predicting repeatedly-scanned samples.

Figure 6. NIR predicted oil concentration against the oil reference chemistry. Since both spectral and reference criteria were used to identify outlying samples, some points that appear to be well predicted were removed because of their excessively high influence on the model (according to 95% Hotellings T^2 confidence limit).

kernels, ranging in moisture content from 3.8% to 40.1%. While their SECV would likely have been somewhat lower, it should be noted that their study was performed using samples of only one hybrid and growing season. As Finney and Norris suggest, the single-kernel moisture reference method may be limiting the perceived performance of moisture prediction by NIR.

In every test, PCR performed slightly worse than PLS. However, the stability of PCR prediction was far superior to that of PLS. Given that the difference in SECV of the two methods is inconsequential, the more stable model would likely be a better choice for making future predictions. Examination of the PLS and PCR regression vectors shows that the PCR vector exhibits somewhat lower frequency variation, while following basically the same trend (fig. 4). A smoothed version (using an adaptive smoothing kernel) of the PCR regression vector (fig. 5) aids interpretation of the moisture calibration; some of the peaks could be positively identified as being related to the major constituents in maize, especially protein at 910 nm and water at around 960-970 nm (Williams and Norris, 1987; Osborne et al., 1993). Not surprisingly, during an ad hoc test, the smoothed version of the regression vector performed better in prediction than did the original.

OIL CALIBRATION RESULTS

The results for the oil calibration tests were worse than those for the moisture calibration (table 3). While some preprocessing had a positive effect on calibration performance, SNV in particular, even the best results obtained were hardly useful. Visually, though, the calibration appears to have some potential (fig. 6). With the removal of a bit more suspect data, model performance should increase quickly. However, in this case, no quantitative rationale could be made to justify removing more outliers (all prediction residuals were within 95% confidence limits). Furthermore, while some samples (marked as outliers) appear to be well predicted, they were omitted from the model because their model influence exceeds the 95% multivariate confidence limit (Hotellings T^2).

The oil calibration results were much worse than those reported by Orman and Schumann (1992), who observed an SECV of 1.30% oil, and a coefficient of determination of 0.75 for their single-kernel oil calibration. Their calibration was built using a much larger calibration database (930 samples), and they utilized nuclear magnetic resonance (NMR) spectroscopy for the oil chemistry reference assay. They did not find NIR spectroscopy to be as effective as NMR spectroscopy for quantifying single-kernel oil content, which has demonstrated a very high correlation (r = 0.99) with solvent extraction (Alexander et al., 1967). However, they suggest that NIR spectroscopy has great untapped potential in that it can be used to simultaneously quantify other species (such as starches) important to the quality of maize kernels. Indeed, NIR imaging spectroscopy could add the potential to capture the distribution of constituents in seeds, as well as identify morphological defects.

In light of the poorer performance of the oil calibration, an experiment was conducted to estimate the contributions to model error from the reference chemistry, the spectrometer, and the calibration, according to the following model:

$$MSE_{total} = [MSE_1 + MSE_2] + [MSE_3 + MSE_4] \quad (3)$$

where

MSE_{total} = total mean squared error of the best model = 1.96

MSE_1 = reference chemistry repeatability (ground grain samples) = 0.72

MSE_2 = difference in mean squared error between extracting oil from bulk ground grain and single-kernel samples >= 0

MSE_3 = mean squared error of the spectrometer repeat ability = 0.30

MSE_4 = mean squared calibration error.

To determine MSE_1, the percentage of oil concentration was determined for eight 0.3 g samples drawn from each of five lots of ground maize. The same method was used as for the single-kernel oil reference chemistry, except without crushing and grinding by mortar and pestle. The purpose of MSE_2 is to account for the difference between mortar and pestle grinding and machine grinding. In this case, it is conservatively assumed that MSE_2 approximately equals 0. The square of the stability (RMSE) measurements for the oil calibration were used for MSE_3. Solving equation 4 for MSE_4 showed that calibration error and reference chemistry error accounted for nearly 50% and 40% of the model error, respectively. If it is assumed that that calibration error will tend to track the error in reference chemistry, and if the oil reference error could at least approach the accuracy attained in bulk oil analyses (MSE ~ 0.026), then standard errors of prediction approaching 0.65 (% oil) are achievable using the hyperspectral imaging spectrometer (assuming no change in instrument repeatability, using equation 3).

It is reasonable to assume that both the moisture and oil reference chemistry methods used are more erroneous (than the bulk methods) for two reasons: (1) inaccuracy in measuring loss-in-weight due to balance errors and human error are much larger relative to the mass of a single-kernel sample, and (2) since the entire sample is destroyed in collecting only one reference analysis, there is no possibility of averaging repeated measurements to decrease noise and to detect anomalies. With this in mind, it would be advisable to collect a very large and diverse calibration database so that reference error can be overcome by volume, or utilize a more accurate or nondestructive reference method, such as NMR, for single-seed analysis.

CONCLUSIONS

Based on the results of this study, the following conclusions can be made:

- Single-kernel analysis by hyperspectral NIR imaging may be a useful technique for quantitative prediction of the moisture concentration of single kernels of maize, but was not useful in predicting oil content. A major portion of the error in the oil calibration was attributable to the reference method rather than the spectrometer. While the objective of this work was to develop techniques for calibrating an imaging spectrometer for quantitative prediction, not necessarily to replace other methods of single-seed oil content analysis, the technique is in need of further refinement before more difficult applications can be approached.

- SNV and detrending may be useful in preprocessing NIR spectra gathered using the hyperspectral imaging spectrometer. Multiplicative scatter correction was not useful in processing spectra in any these experiments.

- Data reduction by genetic algorithm did not improve calibration performance for either the moisture or oil calibrations. It did not significantly reduce performance, however, which suggests that it may have some use in reducing the time required to collect and process sample scans.

FURTHER RESEARCH

Although the objectives of this work were achieved satisfactorily, significant further research efforts are needed before the imaging spectrometer will be a viable technology for quantitative single-seed analysis. Given the results shown here, future research efforts will focus on three areas for improving the utility of the imaging spectrometer:

- Drawing on the fields of spectroscopy, chemometrics, and image analysis, better methods of including the spatial component of the data into calibration and prediction methods are needed. Some possibilities might include pre-classifying the various regions of each kernel using their spectral data and image processing operations; multiple models could be applied, each being specific to a different region of the kernel. Another strategy might be to develop nonlinear models that use the size and shape of kernel regions, as well as spectral data, as inputs for predictions. It is hoped that the utility of the imaging spectrometer will ultimately not be in predicting major constituents like oil (which may be sufficiently well analyzed via other means) but rather in detecting much finer structures (e.g., amino acids, fatty acids, etc.). Since these features are also likely to be heterogeneously distributed within each kernel, an imaging method may have a sensitivity advantage by locating regions of locally high concentration.

- The signal-to-noise ratio must be improved before quantitative calibrations can be deployed. Current research efforts are focusing on using standards placed in the field of view to help mitigate the impact of short and long term variations in the system.

- Future calibration efforts must include improvements to the method of gathering chemical reference data.

REFERENCES

AACC. 1999. AACC method 39-00: Near-infrared methods: Guidelines for model development and maintenance. In *Approved Methods of the American Association of Cereal Chemists*, 10th ed. St. Paul, Minn.: AACC.

Abe, H., T. Kusama, S. Kawano, and M. Iwamoto. 1995. Non-destructive determination of protein content in a single kernel of wheat and soybean by near-infrared spectroscopy. In *Near-Infrared Spectroscopy: The Future Waves*, 457-461. A.

M. C. Davies and P. Williams, eds. Chichester, U.K.: NIR Publications.

Alexander, D. E., L. Silvela, F. I. Collins, and R. C. Rodgers. 1967. Analysis of oil content of maize by wide-line NMR. *J. American Oil Chem. Soc.* 44: 555-558.

AOCS. 1993. AOCS method AM 3-96: Supercritical fluid extraction. In *Official Methods and Recommended Practices of the American Oil Chemists Society*, 4th ed., 3rd printing. Champaign, Ill.: AOCS.

Archibald, D. D., C. N. Thai, and F. E. Dowell. 1998. Development of short-wavelength near-infrared spectral imaging system for grain color classification. *Proc. SPIE* 3543: 189-198.

ASAE Standards, 44th ed. 1997. ASAE Standard S352.2: Oven temperature and heating period for moisture content determinations. St. Joseph Mich.: ASAE.

Barnes, R. J., M. S. Dhanoa, and S. J. Lister. 1989. Standard normal variate transformation and de-trending of near-infrared diffuse reflectance spectra. *Applied Spectroscopy* 43(5): 772-777.

Bellon, V., G. Rabatel, and C. Guizard. 1992. Automatic sorting of fruit: Sensors for the future. *Food Control* (Jan.): 49-54.

Evans, M. D., C. N. Thai, and C. J. Grant. 1998. Development of a spectral imaging system based on a liquid crystal tunable filter. *Trans. ASAE* 41(6): 1845-1852.

Finney, E. E., Jr., and K. H. Norris. 1978. Determination of moisture in corn kernels by near-infrared transmittance measurements. *Trans. ASAE* 21(3): 581.

Geladi, P., and B. R. Kowalski. 1986. PLS Tutorial. *Anal. Chim. Acta* 185(1): 1-17.

Geladi, P., and H. Grahn. 1996. *Multivariate Image Analysis*. New York, N.Y.: John Wiley and Sons.

Goldberg, D. E. 1989a. *Genetic Algorithms in Search, Optimization, and Machine Learning*. Reading, Mass.: Addison-Wesley.

Goldberg, D. E. 1989b. Sizing populations for serial and parallel genetic algorithms. In *Proc. 3rd International Conference on Genetic Algorithms*, 70-79. San Mateo, Cal.: Morgan Kaufmann.

Hardy, C. L., G. Rippke, C. R. Hurburgh, Jr., and T. J. Brumm. 1996. Calibration and field standardization of Foss Grainspec Analyzers for corn and soybeans. In *Near-Infrared Spectroscopy: The Future Waves*, 122-131. A. M. C. Davies and P. Williams, eds. Chichester, U.K.: NIR Publications.

Hatem, I., J. Tan, and P. Shatadal. 1999. Beef quality prediction by using near-infrared image features. Presented at the 1999 ASAE/CSAE-SCGR Annual International Meeting. ASAE Paper No. 993159. St. Joseph. Mich.: ASAE.

Lamb, D. T., and C. R. Hurburgh, Jr. 1991. Moisture determination in single soybean seeds by near-infrared transmittance *Trans. ASAE* 34(5): 2123-2129.

Liu, J. 2001. Design and implementation of real-time image acquisition and processing systems. MS thesis. Ames, Iowa: Iowa State University.

Martens, H., and T. Næs. 1989. *Multivariate Calibration*. New York, N.Y.: John Wiley and Sons.

Miller, B. K., and M. J. Delwiche. 1990. Spectral analysis of peach surface defects. ASAE Paper No. 906040. St. Joseph, Mich.: ASAE.

Miller, P. J., and C. C. Hoyt. 1995. Multispectral imaging system with a liquid crystal tunable filter. *Proc. SPIE* 2345: 354-365.

Næs, T., and H. Martens. 1988. Principal component regression in NIR analysis: Viewpoints, background details, and selection of components. *J. Chemometrics* 2: 155-167.

Norris, K. H. 1983. *Food Research and Data Analysis*, 95-113. H. Martens and H. Rasswum, Jr., eds. New York, N.Y.: Applied Sciences Publishers.

Norris, K. H., and J. R. Hart. 1965. Direct spectrophotometric determination of moisture content of grain and seeds. In *Principles and Methods of Measuring Moisture in Liquids and Solids, Vol. 4: Proc. 1963 International Symposium on Humidity and Moisture*, 19-25. New York, N.Y.: Reinhold Publishing.

Orman, B. A., and R. A. Schumann, Jr. 1992. Nondestructive single-kernel oil determination of maize by near-infrared transmission spectroscopy. *J. American Oil Chem. Soc.* 69: 1036-1038.

Osborne, B. G., T. Fearn, and P. H. Hindle. 1993. *Practical NIR Spectroscopy*. 2nd ed. New York, N.Y.: Longman Scientific and Technical.

Park, B., R. Chen, and M. Nguyen. 1998. Multi-spectral image analysis using neural network algorithm for inspection of poultry carcasses. *J. Agric. Eng. Research* 69(4): 351-363.

Patrick, B. E., and G. D. Jolliff. 1997. Nondestructive single-seed oil determination of meadowfoam by near-infrared transmission spectroscopy. *J. American Oil Chem. Soc.* 74: 273-276.

Ridgeway, C., and J. Chambers. 1998. Detection of insects inside wheat kernels by NIR imaging. *J. Near-Infrared Spectroscopy* 6: 115-119.

Roussel, S. A., C. L. Hardy, C. R. Hurburgh, Jr. and G. R. Rippke. 2001. Detection of Roundup Ready soybeans by near-infrared spectroscopy. *Applied Spectroscopy* 55(10): 1425-1429.

Sato, T., Y. Takahata, T. Noda, T. Yanagisawa, T. Morishita, and S. Sakai. 1995. Nondestructive determination of fatty acid composition of husked sunflower seeds by near-infrared spectroscopy. *J. American Oil Chem. Soc.* 72: 1177-1183.

Sato, T., I. Uezono, T. Morishita, and T. Tetsuka. 1998. Nondestructive estimation of fatty acid composition in seeds of *Brassica napus* L. by near-infrared spectroscopy. *J. American Oil Chem. Soc.* 75: 1877-1881.

Silvela, L., R. Rodgers, A. Barrera, and D. E. Alexander. 1989. Effect of selection intensity and population size on percent oil in maize. *Theoretical and Applied Genetics* 78: 298-304.

Sugiyama, J. 1999. Visualization of sugar content in the flesh of a melon by near-infrared imaging. *J. Agric. and Food Chem.* 47(7): 2715-2718.

Tang, L., L. Tian, and B. L. Steward. 2000. Color image segmentation with genetic algorithm for in-field weed sensing. *Trans. ASAE* 43(4): 1019-1027.

Taylor, S., and W. F. McClure. 1989. NIR imaging spectroscopy: Measuring the distribution of chemical components. In *Proc. 2nd International Near-Infrared Spectroscopy Conference*, 393-404. Tokyo, Japan: Korin Publishing.

Upchurch, B. L., J. A. Throop, and D. J. Aneshansley. 1994. Influence of time, bruise type, and severity on near-infrared reflectance from apple surfaces for automatic bruise detection. *Trans. ASAE* 37(5): 1571-1575.

Velasco, L., B. Pérez-Vich, and J. M. Fernández-Martinez. 1999a. Nondestructive screening for oleic and linoleic acid in single sunflower achenes by near-infrared reflectance spectroscopy. *Crop Science* 39: 219-222.

Velasco, L., C. Möllers, and H. C. Becker. 1999b. Estimation of seed weight, oil content, and fatty acid composition in intact single seeds of rapeseed by near-infrared reflectance spectroscopy. *Euphytica* 106(1): 79-85.

Velasco, L., C. Möllers, and H. C. Becker. 1999c. Screening for quality traits in single seeds of rapeseed by near-infrared reflectance spectroscopy. In *New Horizons for an Old Crop: Proc. 10th International Rapeseed Congress*. N. Wratten and P. A. Salisbury, eds. Canberra, Australia: The Regional Institute.

Williams, P., and K. Norris. 1987. *Near-Infrared Technology in the Agricultural and Food Industries*, 247-290. St. Paul, Minn.: American Association of Cereal Chemists.

Wold, S., A. Ruhe, H. Wold, and W. J. Dunn III. 1984. The collinearity problem in linear regression: The partial least squares approach to generalized inverses. *SIAM J. Sci. and Stat. Computing* 5(3): 735-743.

Zwiggelaar, R., Q. Yang, P. Garcia, and C. R. Bull. 1996. Use of spectral information and machine vision for bruise detection on peaches and apricots. *J. Agric. Eng. Research* 63(4): 323-331.